AIMS Materials Science, 5(3): 519–532.
DOI: 10.3934/matersci.2018.3.519
Received: 27 April 2018
Accepted: 24 May 2018
Published: 28 May 2018

http://www.aimspress.com/journal/Materials

Research article

Nanocrystalline diamond coatings: Effects of time modulation bias enhanced HFCVD parameters

Abbas Hodroj[1], Lionel Teulé-Gay[1], Michel Lahaye[2], Jean-Pierre Manaud[1] and Angeline Poulon-Quintin[1,*]

[1] CNRS, Université de Bordeaux, ICMCB, UMR 5026, F-33600 Pessac, France
[2] Université de Bordeaux, Placamat, UMS 3626, F-33600 Pessac, France

* **Correspondence:** Email: angeline.poulon@icmcb.cnrs.fr; Tel: +33540002650; Fax: +33540002761.

Abstract: Nanocrystalline diamond NCD coatings could improve the performances of cutting tools if the adhesion on cobalt-cemented tungsten carbide WC–Co substrates was optimized and maintained during diamond deposit. In this study, a time modulated polarized growth process during diamond hot filament chemical vapor deposition (HFCVD) method was used. NCD coatings were deposited on cobalt-cemented tungsten carbide (WC–10% Co) substrates previously coated with tantalum or zirconium nitride–molybdenum bilayer as interlayer systems to control carbon and cobalt diffusion. Continuous films consisted of diamond clusters. Their size decreased when the applied bias voltage increased and substrate temperature decreased. Raman analyses confirmed the reduction of crystallite size and formation of nanocrystalline diamond films by time modulated biased substrate HFCVD process. Scratch tests showed that the NCD/interlayer systems/WC–10% Co displayed very good film adhesion interesting for cutting tools applications compared to NCD/WC–10% Co. In addition using an interlayer system could offer additional protection when diamond coating was deteriorated. This technique seems to be promising for industrial applications in the field of machining tools when increasing the thickness of the diamond layer by only extending the time modulated deposition process.

Keywords: NCD; HFCVD; time modulated polarized growth; Raman; AES; adhesion

Abbreviations: AES: Auger Electron Spectrometry; BSE: BackScattered Electron; CCD: Cooled Charge-coupled Device detector; CVD: Chemical Vapor Deposition; DCCVD: Direct Current

plasma Chemical Vapor Deposition; EDS: Energy Dispersive X-ray Spectrometer; HFCVD: Hot Filament Chemical Vapor Deposition; MWCVD: Micro Wave enhanced Chemical Vapor Deposition; NCD: NanoCrystalline Diamond; SEM: Scanning Electron Microscope; XRD: X-Ray Diffraction

1. Introduction

In the last few years, nanocrystalline diamond (NCD) films have emerged as interesting materials for engineering applications because of its useful mechanical, optical, thermal and electrical properties [1–6]. The combination of the high hardness with low surface roughness makes NCD coatings ideal for an improved performance of cutting tools [7–10]. However, presence of cobalt binder inside WC–Co tools, is damageable for the diamond coating adhesion. Cobalt is well known to prevent the diamond growth and to enhance the formation of the graphitic species [11,12]. In order to avoid the diffusion of cobalt up to the free surface where diamond could be formed, different methods are used: (1) low or high depth chemical etching to remove the cobalt from the surface of WC–Co tool [13,14] which unfortunately weakens the surface mechanical properties of these cemented carbides; (2) the use of Co diffusion barrier interlayers [15–18]. Metallic nitrides (TaN and ZrN) coatings are already shown to be efficient as Co diffusion barrier [17,18]. Nevertheless, the diamond nucleation density on metallic nitrides or carbides is lower compared to that obtained from their forming pure metal [19] as pure molybdenum [20]. The TaN and ZrN diffusion barriers are then coated with a thin Mo nucleation layer in order to develop useful bilayer interlayer systems able not only to avoid the Co diffusion from the WC–Co surface but also to monitor the carbon diffusion during diamond deposition [18]. A chemical diffused interface is expected between WC–Co substrate and diamond layer letting hope for an increase of diamond layer adhesion.

NCD films are deposited by various CVD methods such as hot filament CVD (HFCVD) [20–23], direct current plasma CVD (DCCVD) [24], plasma enhanced CVD (PECVD) [25] and microwave plasma enhanced CVD (MWCVD) [3,26]. By changing the standard CVD deposition parameters such as gas mixture, pressure, substrate temperature, and by applying a continuous substrate bias [23,26–28], the morphology and the microstructure of diamond could be modified. NCD might be obtained. We have shown that during MWCVD diamond growth, the time modulated biased substrate process, leads to produce NCD coatings consisting of multilayer clusters composed of two alternating diamond nanograin sizes [29]. The HFCVD process is relatively cheap and easy to operate to get low cost diamond films for tooling applications in comparison to other plasma based CVD techniques. We intend to study the influence of time modulated negative substrate polarization process during HFCVD diamond deposition. This paper focuses on the effect of this modulated polarization on the morphology and on the structure of diamond coatings deposited on WC–Co substrate previously coated with TaN–Mo or ZrN–Mo bilayer systems. The adhesion behavior of diamond coatings to the bilayer systems and the substrate is also investigated for a selected set of HFCVD process parameters promising in terms of low graphitic species content.

2. Materials and method

2.1. Interlayer deposition

Cobalt diffusion barrier such as TaN or ZrN and Mo nucleation layer were deposited on WC–10%

Co substrate disks (16 mm in diameter, 3 mm thick) by reactive magnetron sputtering process in a Plassys MP700 sputtering chamber baked via mechanical and turbo-molecular pumps. The base pressure prior to the deposition was in the range of 2–3 × 10^{-5} Pa. The total pressure during the deposition process was 0.5 Pa. The vacuum chamber of the plant was equipped with five radio frequency (13.56 MHz) magnetrons, 75 mm in diameter targets and an ion source (Anatech IS 3000). The distance from the magnetron source to the substrates was 7 cm. Deposition of interlayers was performed with additional heating of substrates up to 723 K measured by a thermocouple. Prior to deposition, cemented carbide substrates were blasted with alumina micro particles, cleaned ultrasonically in acetone. They are rinsed using isopropanol vapor before interlayer deposition. Just before deposition, the cleaning procedure was completed by in-situ etching thanks to a high energy argon ion beam surface treatment (50 eV, 0.02 Pa, 10 min).

For nitride and molybdenum layers (respectively 1 and 0.5 μm of thickness, Figure 1a), Ta, Zr and Mo metallic targets were used as sputter sources. The power density applied to the Ta, Zr and Mo sputter target was 2.3, 4 and 2.3 W cm^{-2}, respectively. The deposition reactive environment was a nitrogen/argon atmosphere with overall flow rate of 50 sccm. The total pressure was kept at 35 hPa. The nitrogen/argon ratio was set at 10% for TaN and 6% for ZrN, respectively. The growth rate was calculated to be 10, 16 and 20 nm/min for TaN, ZrN and Mo films, respectively.

2.2. Diamond deposition

Diamond thin films were deposited on interlayer system coating WC–10% Co substrates using a hot filament CVD method. Prior to their introduction in the HFCVD chamber, the coated substrates were seeded during 1 hour by ultrasonic agitation using 100 nm polycrystalline diamond suspensions in order to overcome the typical low diamond nucleation density on hetero-materials.

The HFCVD setup included a deposition chamber and a monitored blending system able to mix up to four gases (H_2, CH_4, Ar and He). Ultra-pure H_2 was obtained from a Parker hydrogen generator. The other gases were Alphagaz 2 grade. The chamber included a sample holder (cathode) that may be sequentially negatively polarized by a high voltage supplier and heated, a grounded anode and the tungsten filaments (0.45 mm in diameter) powered thanks to a DC generator. All these components were monitored by a computer. Filament and substrate temperatures were measured by two independent bi-band Raytek optical pyrometers.

During the process the overall pressure of blended gases was kept constant. All the samples were heated thanks to filament heat radiation up to 1000 or 1100 K in an argon/hydrogen atmosphere to avoid oxidation during half an hour. The filament carburization step consisted in increasing the temperature of filaments by passing DC current through them, reaching their temperatures of 2673 K under a rich CH_4 atmosphere [CH_4/H_2 mixture (3% of CH_4)] with the substrates in position. Then the diamond synthesis was carried out in two additional steps (WO/2010/076423 patent [30]) keeping the sample temperature equal to 1000 or 1100 K (Figure 1b):

(1) A diamond nucleation period in a methane rich CH_4/H_2 mixture (3% of CH_4) for 30 min without any polarization. According to [19,21], the solubility of carbon in Mo and Mo carbide formation increase the nucleation density and contributes to limit the size of diamond grains and to start an heterogeneous diamond nucleation.

(2) A sequenced polarized growth period under 1% CH_4 in H_2. The diamond was firstly grown during t min without using any substrate bias. Then a negative bias (−200 or −300 V) was applied to

the substrate for t/3 min. Application of the negative bias led to a substrate temperature increase of 10–20 K. This time modulated negative substrate polarization method was repeated during the sequenced polarized growth period (global duration 4 h) in order to limit the columnar growth of grains and their coalescence. In addition as the mean free path of the species at the operating pressure was very short, etched carbon and carbon species may be redeposited and so might enhance a secondary diamond nucleation. As a consequence diamond films were expected nanocrystalline and smooth.

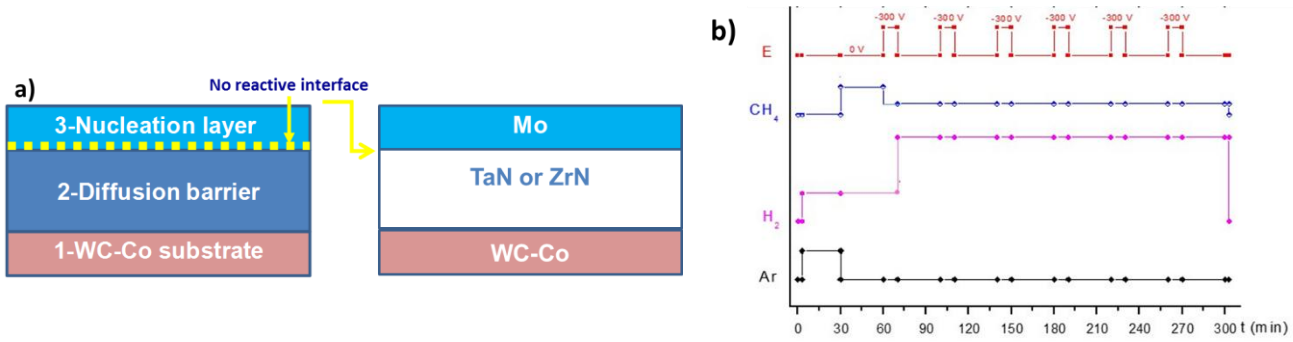

Figure 1. Schema of the interlayers used before diamond deposit (a) and an example of time diagram of the CVD process (gases and bias value sequences) (b).

2.3. Characterizations

The surface morphology of the samples was observed with a Jeol JMS 6360A scanning electron microscope (SEM) equipped with an energy dispersive X-ray spectrometer (EDS). X-ray diffraction (XRD) experiments were carried out on a θ/2θ Philips PW1820 powder diffractometer (Cu $K_{\alpha 1}$, λ = 0.15406 nm). Raman spectra were collected using a Jobin Yvon/Horiba LabRam HR800-UV spectrometer equipped with a Peltier cooled charge-coupled device (CCD) detector. Experiments were carried out in the micro-Raman mode at room temperature in a backscattering geometry. The 514.5 nm line of an Ar^+ laser was focused to a spot size smaller than 2 μm. The incidence laser beam power measured on the sample surface was close to 50 mW. Elemental depth profiles were obtained by Auger Electron Spectrometry (AES VG Scientific Microlab 310F, 10 keV, 5 nA) coupled with argon etching (4.5 keV, 400 nA). The elemental atomic concentration was estimated from the energy peaks spectrum in correlation with AES database. In order to determine the carbon Auger line shapes resulting from diamond component, the carbon Auger spectrum was deconvoluted into C–C (diamond or graphite) or free carbon and C–metal (carbide) signals by using factor analysis methods.

Scratch tests were performed using a Tribotechnic Millenium 100 scratch-tester under Standard ISO/EN 1071-3. A Rockwell C diamond tip indenter with a 200 nm radius of curvature was drawn during the scratch test over the coated surface for 10 mm-length with an applied normal load increased continuously up to 50 N. The tip wear was controlled between each measurement. An acoustic sensor allowed to record the cracks threshold. The surface of the scratched samples was subsequently observed with SEM-EDS in order to provide information on the localization of the cracks or spalling beginning.

3. Results and discussion

3.1. Morphology and structure

Top surface aspect of diamond films deposited on WC–10% Co substrates coated with TaN–Mo interlayers are shown in Figure 2. The diamond morphology depends on the substrate temperature and on the biasing conditions during time modulated polarized growth step and does not depend on the bilayer system used.

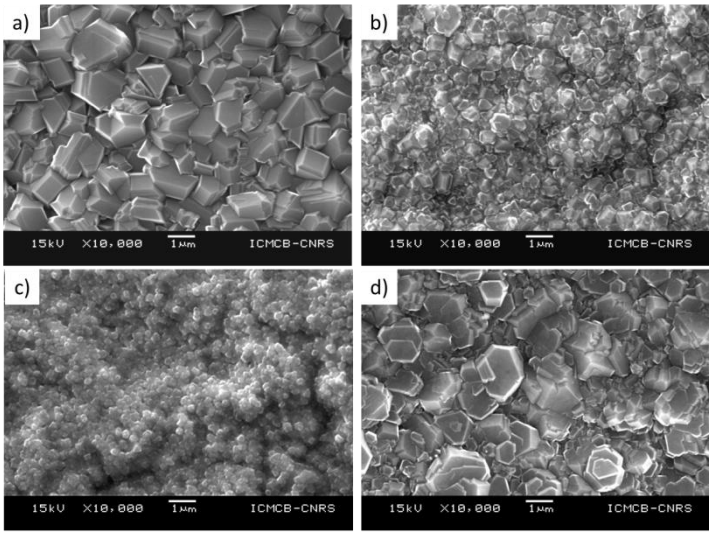

Figure 2. SEM micrographs of the HFCVD diamond film top surfaces deposited on WC–10% Co substrates coated with TaN–Mo bilayer system at various substrate temperatures and applied bias voltages during the time modulated polarized growth step: (a) 1000 K, 0 V; (b) 1000 K, −200 V; (c) 1000 K, −300 V; (d) 1100 K, −300 V.

For substrate temperature of 1000 K and without bias application, a typical microcrystalline diamond (Figure 2a) with faceted grains (~1.5 µm) was obtained. The film thickness estimated on cross section was about 1.5 µm. With −200 V as bias value, the film surface was composed of diamond clusters (Figure 2b, average size of 0.7 µm) and the film thickness was reduced down to 0.5 µm. With the increase of the negative bias value to −300 V, both the cluster size (Figure 2c, average size of 0.2 µm) and the film thickness (0.3 µm) were reduced. The reduction in cluster size and thickness could be attributed to the hydrocarbon–hydrogen species reactive etching of the growing diamond resulting from sequenced negative bias [31]. These clusters were surrounded by tiny ball-like diamond grains. These small-sized diamond polycrystallites could be formed due to the secondary nucleation enhanced by substrate bias application. By increasing the substrate temperature up to 1100 K with increasing the filaments temperature, the films deposited under a bias voltage of −300 V (Figure 2d) showed a mixture of clusters with a size in the range of 0.5–1.5 µm. The increase in filament temperature enhances the dissociation of molecular hydrogen into atomic hydrogen. This activates the reaction with hydrocarbons to facilitate the formation of free radicals such as CH_3 and C_2H_2 which are considered important for diamond growth. This enlargement of the clusters due to the increase of the substrate surface temperature could also be explained by a higher diamond growth

rate [32] and/or for the diamond grains in contact to the interface, to the formation of different types of Mo or Ta carbides.

The θ/2θ X-ray diffraction patterns of TaN–Mo bilayer system without and with diamond films deposited at different bias voltages and substrate temperatures are shown in Figure 3.

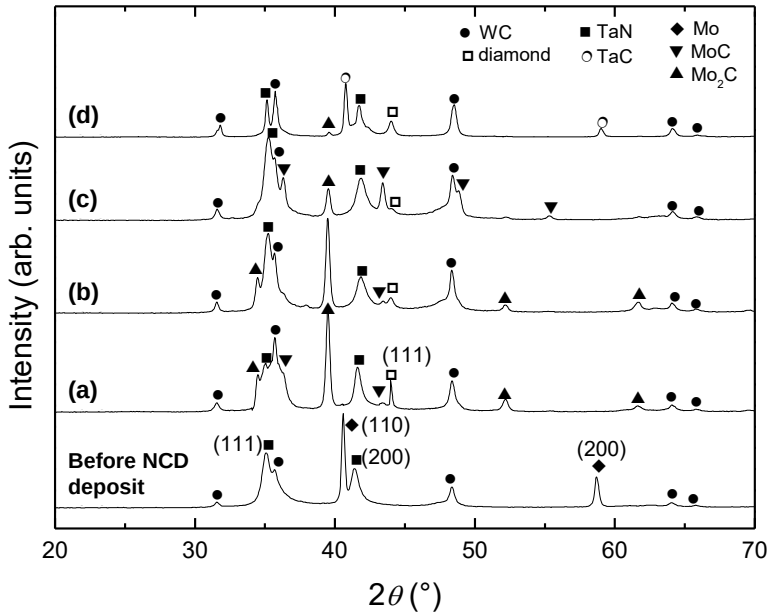

Figure 3. X-ray diffraction patterns of TaN–Mo bilayer system obtained on WC–10% Co substrates before diamond deposition and after diamond growth at different deposition temperatures and substrate bias during the sequenced polarized growth step: (a) 1000 K, 0 V; (b) 1000 K, −200 V; (c) 1000 K, −300 V; (d) 1100 K, −300 V.

The WC peaks corresponding to substrate are always observed. Before diamond deposition, the TaN film crystallizes in fcc-like structure (JCPDS 00-049-1283) while the Mo layer consists in bcc phase (JCPDS 00-042-1120). After diamond grown at 1000 K and without bias (Line a), the TaN and Mo reflections vanish and new peaks assigned to MoC (JCPDS 03-065-3494) and Mo_2C (03-065-8766) phases emerge. The carburization of Mo leads to a fast accumulation of carbon at the surface which promotes diamond nucleation and growth [20]. The peak close to 43.9 °is assigned to the (111) reflection of diamond (JCPDS 00-006-0675) and related to presence of the faceted microcrystalline grains illustrated earlier by SEM (Figure 2). The main change observed at 1100 K when negative bias is applied (Lines b and c, respectively), is the linewidth of (111) diamond reflection, much broader than without bias, indicating a reduction in diamond grain size contained in the multilayered clusters. At 1100 K and −300 V applied bias (Line d), additional peaks corresponding to TaC phase are observed (JCPDS 03-065-8264), suggesting a partial carburization of TaN as previously reported on MWCVD diamond growth [17,18], where the increase in concentration of hydrocarbon species which assumed near top TaN surface accelerates the chemical conversion of nitride into carbide. Only the presence of Mo_2C carbide is noticed. In this study, for HFCVD, this carburization could be related to: (1) the modification of thermodynamic equilibrium with the temperature increase, (2) the enhancement of methane dissociation allowing more production of reactive hydrocarbon species and (3) the increase of solubility and diffusion rates of

carbon with temperature changing the type of carbides obtained and so the diamond nucleation density [33]. Furthermore, the diamond (111) diffraction peak was better defined and not significantly overlapped with MoC peak compared to that obtained at 1000 K. The average size of diamond crystallites included within the clusters, was roughly estimated from the Scherrer's formula to be about 25 nm (within uncertainty of 10%). The clusters consist of alternating diamond layers of two different crystallite sizes, depending on the modulated polarization and according to the multilayer diamond structure produced by using biased sequenced CVD [29]. The estimated crystallite size was their average value.

When ZrN–Mo bilayer system is used, diamond peak behavior is unchanged. The carburization of Mo occurred while ZrN was stable even at 1100 K. It is consistent with that already observed in MWCVD diamond deposition [17]. At this temperature, ZrN is thermochemically stable against methane carburization [17].

Raman analyses are performed to obtain further information on the diamond structure evolution. Figure 4 displays Raman spectra of diamond films grown under different applied bias voltages and temperatures. To bring a better characterization of the film compositions and to determine the number of bands included in the range 800–2000 cm^{-1}, the spectra are deconvolved. The backgrounds of the spectral lines are corrected and fitted using a mixed Gaussian–Lorentzian deconvolution procedure.

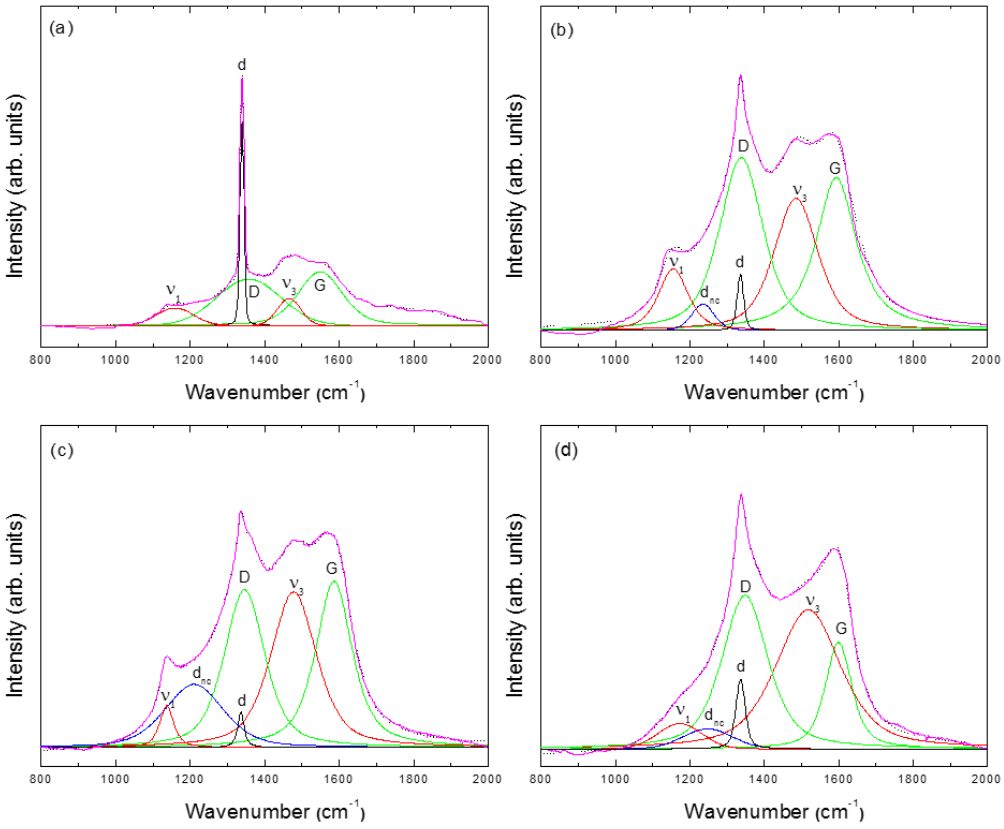

Figure 4. Mixed Gaussian–Lorentzian deconvolution of the measured Raman spectra of diamond films deposited at different substrate temperatures and applied bias voltages during the time modulated polarized growth stage: (a) 1000 K, 0 V; (b) 1000 K, −200 V; (c) 1000 K, −300 V; (d) 1100 K, −300 V.

For 1000 K and 0 V, the deconvolution provides five overlapping bands centered at 1158, 1336, 1356, 1465 and 1550 cm^{-1}, whatever the bilayer systems (TaN–Mo or ZrN–Mo) used. The sharp band at 1336 cm^{-1} (denoted by "d") was close to that of the first-order optical phonon mode of natural diamond line which appeared at 1332.5 cm^{-1}. This shift might be due to a build-up of compressive stress in the coating and identified as a signature of good adhesion of the film on the substrate [34]. Contributions at 1356 and 1550 cm^{-1} are attributed to D- and G-modes of amorphous carbon [35,36]. The bands at 1158 and 1465 cm^{-1} could correspond to υ_1 (C–H in plane bending combined with C–C stretching) and υ_3 (C=C stretching) Raman modes of trans-polyacetylene (t-PA) segments [37,38] which are mainly present at grain boundaries. These bands are widely assigned to presence of nanometer sized diamond crystals. Their weak intensities indicate a low fraction of grain boundaries and fewer hydrocarbons contained in these boundaries. At −200 V applied bias, the diamond peak became broadened and its intensity decreased strongly suggesting a reduction in the diamond crystallite size. An additional band at about 1235 cm^{-1} (denoted by "d_{nc}") is noticed through fitting procedures that might be interpreted as a vibrational density of states (VDOS) of small diamond crystallites [39,40]. The intensity ratio of the diamond peak to that of VDOS feature (I_d/I_{dnc}) could be used to evaluate the nanocrystallinity of diamond [41]. If the crystallite size is lower than 10 nm, this ratio falls to zero (diamond peak is completely vanished). By decreasing the substrate bias to −300 V at the same temperature (1000 K), the I_d/I_{dnc} ratio decreases (Table 1) indicating further diminishing of nanocrystallite size to values remaining above 10 nm. On the contrary, rising the substrate temperature to 1100 K leads to increase this ratio suggesting that the nanocrystallites are enlarged. The relative amount of trans-polyacetylene like material in the grain boundaries can be evaluated from the intensity ratio of the υ_1 (t-PA) band versus the G one, $I_{t\text{-}PA}/I_G$ [40]. When negative bias decreased from −200 to −300 V, a drop in this ratio is observed indicating a reduction of contained t-PA-like material (sp^2 C formed on the grain boundaries) under CH_4/H_2 ion bombardment during modulated polarization (Table 1). The intensity ratio of the D-band to G-band, I_D/I_G, is inversely proportional to the cluster size of the graphite [21] in films. At 1000 K, the graphite size is slightly increased by raising the bias voltage. I_D/I_G values from 0.94 to 1.44 suggest that the state of graphite is nanocrystalline graphite and is not induced by Cobalt [40]. The larger the value of I_D/I_G is, the smaller the content of sp^3 phase is and the larger the content of sp^2 phase is [40]. The decreasing of I_D/I_G ratio with diamond crystallite size is previously reported by Klauser et al. [40] on NCD films grown by unbiased HFCVD. They also observe no significant change in sp^3 grain boundary contents with this increase. In our films, the ion bombardment resulting from sequenced negative bias could slightly increase the deposition temperature, prompting the conversion from sp^2 to sp^3 bonding. Lowest I_D/I_G ratio are noticed for 1000 K, −250 and −300 V bias.

Table 1. I_d/I_{dnc}, $I_{t\text{-}PA}/I_G$, I_D/I_G ratio values derived from the Raman spectra for the NCD films deposited at various substrate temperatures (1000 and 1100 K) and applied bias voltages (−200, −250 and −300 V) during the time modulated polarized growth step.

Substrate temp. (K)	Substrate bias (V)	I_d/I_{dnc}	$I_{t\text{-}PA}/I_G$	I_D/I_G
1000	−200	2.13	0.40	1.13
1000	−250	1.57	0.33	0.95
1000	−300	0.56	0.25	0.94
1100	−300	3.47	0.24	1.44

It is quite clear from Raman results that the decreasing of negative substrate bias during time modulated polarized growth step enhances the formation of nanocrystalline diamond, whereas the increase in the substrate temperature leads to diamond crystallites growth (in agreement with XRD results). In this study, the smaller diamond crystallites, are produced at 1000 K of deposition temperature and −300 V of negative bias.

3.2. Depth profiling and coating adhesion

Based on the Raman analyses, parameters selected to elaborate diamond layer tested in this part are: 1000 K and −300 V. Diamond layers grown present the lowest the diamond size and the highest diamond content. AES analyses are performed to collect information over the depth profiles of C, Mo, Ta (or Zr), N, W and Co in approximately 1.8 μm thick sample (Figure 5, diamond continuous layer: 0.3 μm; bilayer system: 1.5 μm). Before diamond deposition, the bilayer systems TaN–Mo or ZrN–Mo exhibited a quasi-uniform distribution of Ta or Zr and N elements along the TaN or ZrN layer thickness (Figure 5a,b). Neither the diffusion of Mo from nucleation layer nor that of Co from the substrate towards these nitride layers is noticed, as previously reported [18]. After diamond growth, AES profiles confirm XRD observations: (1) for both bilayer systems, Mo carbide layer is formed (Figure 5c,d) and (2) there is no evidence of the formation of carbide in the TaN or ZrN layer even if the carbon diffused in the vicinity of the top nitride layers.

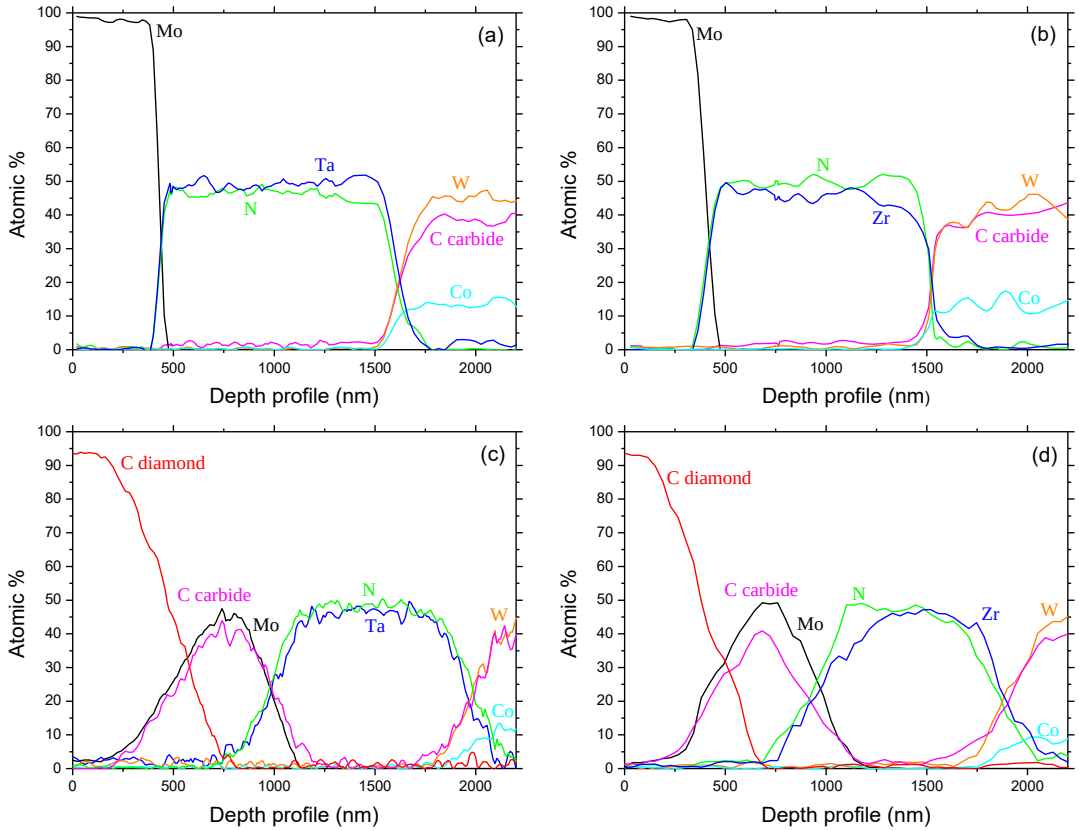

Figure 5. AES depth profiles of TaN–Mo and ZrN–Mo bilayers obtained on WC–10% Co substrates before diamond deposition (a) and (b), and after diamond growth at 1000 K and −300 V applied bias (c) and (d).

To investigate the influence of the interlayer systems on the adhesion of continuous NCD films (0.3 μm thicknesses), scratch tests are performed first on: (1) NCD deposited films (0.3 μm thick) on WC–10% Co coated substrates with TaN–Mo or ZrN–Mo and (2) NCD deposited films (0.3 μm thick) on WC–10% Co without interlayer systems (surface morphology of the diamond films is similar to those obtained with interlayer systems). In this last case, substrates are previously blasted and two step etched in Murakami ($K_3[Fe(CN)_6]$, KOH, H_2O) and Caro (H_2SO_4, H_2O_2, H_2O) solutions to decrease Co content at the surface in contact with diamond and to limit the Co diffusion effect during HFCVD process.

The first peeling off is observed under a critical load of 18.9 ± 0.2 N and 18.4 ± 0.3 N respectively for TaN–Mo and Zr–Mo coated with NCD. The continuous damage appeared at 28.0 ± 0.3 N for TaN–Mo and 28.5 ± 0.1 N for ZrN–Mo. Without interlayer systems, the NCD spalling is started at a relatively low load of few Newton. This weakness in the NCD/substrate interface could be related to the breaking up of the WC grains at substrate surface due to the surface chemical treatment leading to brittle area and delamination by grain shedding. Figure 6 illustrates the BSE-SEM micrographs of scratched typical area at approximately 18.5 N for NCD coated interlayers. Elemental analyses by EDS of this peeled region show the presence in the diamond first peeling area of Ta in the TaN–Mo bilayers case (red/pink color) and of W in the ZrN–Mo one (blue color). With the use of the TaN–Mo system, decohesion occurs at the Mo carbide/TaN interface, whereas in the case of the ZrN–Mo bilayer, the peeling is produced at the ZrN/substrate interface. Therefore, the adhesion of the Mo carbide/ZrN interfaces is stronger than those of the Mo carbide/TaN and ZrN/substrate. However this difference could not be directly related to the thermal expansion coefficient values of substrate and layers. Contrary to TaN which has a thermal expansion coefficient of 3.6×10^{-6} K^{-1}, ZrN presented a coefficient of 7.2×10^{-6} K^{-1} [42] which is nearest to that of WC–10% Co (5.8×10^{-6} K^{-1}) and similar to Mo_2C thermal expansion coefficient (5.1×10^{-6} K^{-1}). This should involve a reduction in residual thermal stress inside ZrN–Mo interlayer systems at the interface with the substrate. Moreover, thermomechanical computation [29] has shown that the addition of a Mo nucleation layer able to be carburized during the CVD process and the capacity of the diffusion layer to be entirely carburized (TaC thermal expansion coefficient: 7.2×10^{-6} K^{-1}) leads to a reduction of the tensile stress values obtained inside the diffusion layer. The change in chemical bonding at interlayer interfaces due to the diffusion of species during diamond deposition is another contribution to the adhesion which could be taken into account. Indeed, a diffusion of carbon near the top nitride layers is observed by AES analyses and TaC formation is noticed on XRD diffractogram. TaN has more tendency to react with carbon, as previously mentioned, allowing change in the chemical bonding and consequently probably weakening of the Mo carbide/TaN interface. However for Rockwell indentation test, spalling of diamond coating at the interface of Ta film and substrate after HFCVD NCD deposit (1050 K without bias) is already attributed to the poor adhesion of TaN to the substrate and the formation of TaC. Authors noticed the golden yellow color of the spalling coating attributed to the carbide presence and confirmed by elemental analyses. In our case, only TEM observation should confirm presence of carbide at the interface with the Mo layer or the substrate.

Until total spalling of the diamond layer, the use of the TaN–Mo bilayer system could offer an additional protection to the WC–Co tool. The first crack occurring at the interface with Mo leads to a surface still protected by TaN or TaC which could impact the duration of a tool compared to a direct exposure of the WC–Co when the ZrN–Mo bilayer system is used.

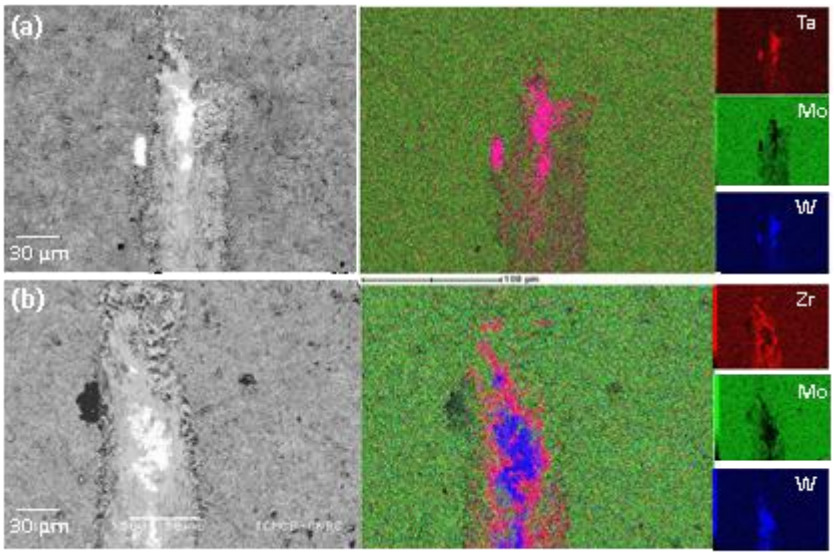

Figure 6. SEM (BSE mode) micrographs and the corresponding EDS overlay maps of the first peeling off area for NCD films deposited at 1000 K and −300 V on WC–10% Co substrates coated with TaN-Mo (a) and ZrN-Mo (b) interlayers.

4. Conclusions

A time modulated negative substrate polarization process during HFCVD technique was used to grow NCD coatings on WC–10% Co previously coated with TaN–Mo or ZrN–Mo bilayer systems. By increasing the bias voltage from −200 V to −300 V, the morphology of coatings grown at 1000 K showed a reduction in cluster size of diamond by 60%. The crystallite size within the clusters was also decreased as deduced from XRD analyses. Raman measurement provided an evidence that the smaller grains were obtained at −300 V by comparing the intensity ratio of the diamond line "d" to the VDOS feature "d_{nc}". From these two techniques, the estimated average crystallite size is ranging between 10 and 20 nm.

The carburization of Mo is confirmed either by XRD and AES analyses. The Co diffusion barrier layer TaN or ZrN is not carburized when the substrate temperature is 1000 K. No diffusion of Co towards the interlayer systems was noticed whatever the deposition conditions. For both TaN–Mo and ZrN–Mo interlayer systems, the adhesion of coatings evaluated by scratch testing showed that the first peeling take place at a critical load of about 18.5 N for 0.3 µm-thick NCD films (1 N for NCD coating without interlayer system). The interface Mo carbide/ZrN exhibits a stronger adhesion with respect to ZrN/substrate and Mo carbide/TaN. These results reveal that the time modulated negative substrate polarization process during HFCVD diamond deposition is very promising for the development of NCD coatings. It will improve the performance of cutting tools if it is combined with the used of an interlayer system especially TaN–Mo which is able to offer an additional protection.

Acknowledgments

This work was supported by "Le Conseil Régional d'Aquitaine (France)".

Conflict of interest

All authors declare no conflicts of interest in this paper.

References

1. Williams OA, Nesladek M, Daenen M, et al. (2008) Growth, electronic properties and applications of nanodiamond. *Diam Relat Mater* 17: 1080–1088.
2. Bruhne K, Kumar KV, Fecht HJ, et al. (2005) Nanocrystalline HF-CVD-grown diamond and its industrial applications. *Rev Adv Mater Sci* 10: 224–228.
3. Philip J, Hess P, Feygelson T, et al. (2003) Elastic, mechanical and thermal properties of nanocrystalline diamond films. *J Appl Phys* 93: 2164–2171.
4. Mazellier JP, Mermoux M, Andrieu F, et al. (2011) Enhanced thermal performances of silicon-on-diamond wafers incorporating ultrathin nanocrystalline diamond and silicon layers: Raman and micro-Raman analysis. *J Appl Phys* 110: 084901.
5. Erdemir A, Fenske GR, Krauss AR, et al. (1999) Tribological properties of nanocrystalline diamond films. *Surf Coat Technol* 120–121: 565–572.
6. Yang W, Auciello O, Butler JE, et al. (2002) DNA-modified nanocrystalline diamond thin-films as stable, biologically active substrates. *Nat Mater* 1: 253–257.
7. Hollman P, Wänstrand O, Hogmark S (1998) Friction properties of smooth nanocrystalline diamond coatings. *Diam Relat Mater* 7: 1471–1477.
8. Olszyna A, Smolik J (2004) Nanocrystalline diamond-like carbon coatings produced on the Si_3N_4–TiC composites intended for the edges of cutting tools. *Thin Solid Films* 459: 224–227.
9. Hu J, Chou YK, Thompson RG, et al. (2007) Characterizations of nano-crystalline diamond coating cutting tools. *Surf Coat Technol* 202: 1113–1117.
10. Nitta Y, Hiroki O, Une K (2005) Cutting performance of a nanocrystalline diamond-coated tool. *New Diam Front Carbon Technol* 15: 195–203.
11. Sein H, Ahmed W, Rego C (2002) Application of Diamond Coatings on Small Dental Tools. *Diam Relat Mater* 11: 731–735.
12. Polini R (2006) Chemically vapour deposited diamond coatings on cemented tungsten carbides: Substrate pretreatments, adhesion and cutting performance. *Thin Solid Films* 515: 4–13.
13. Mallika K, Komanduri R (1999) Diamond coatings on cemented tungsten carbide tools by low-pressure microwave CVD. *Wear* 224: 245–266.
14. Deuerler F, Van den Berg H, Tabersky R, et al. (1996) Pretreatment of substrate surface for improved adhesion of diamond films on hard metal cutting tools. *Diam Relat Mater* 5: 1478–1489.
15. Li YS, Tang Y, Yang Q, et al. (2008) Al-enhanced nucleation and adhesion of diamond films on WC–Co substrates. *Int J Refract Met H* 26: 465–471.
16. Xu Z, Lev L, Lukitsch M, et al. (2007) Effects of surface pretreatments on the deposition of adherent diamond coatings on cemented tungsten carbide substrates. *Diam Relat Mater* 6: 461–466.
17. Manaud JP, Poulon A, Gomez S, et al. (2007) A comparative study of CrN, ZrN, NbN and TaN layers as cobalt diffusion barriers for CVD diamond deposition on WC–Co tools. *Surf Coat Technol* 202: 222–231.

18. Poulon-Quintin A, Faure C, Teulé-Gay L, et al. (2010) Bilayer systems of tantalum or zirconium nitrides and molybdenum for optimized diamond deposition. *Thin Solid Films* 519: 1600–1605.
19. Sarangi SK, Chattopadhyay A, Chattopadhyay AK (2008) Effect of Pretreatment, Seeding and Interlayer on Nucleation and Growth of HFCVD Diamond Films on Cemented Carbide Tools. *Int J Refract Met H* 26: 220–231.
20. Buijnsters JG, Vázquez L, Van Dreumel GWG, et al. (2010) Enhancement of the nucleation of smooth and dense nanocrystalline diamond films by using molybdenum seed layers. *J Appl Phys* 108: 103514.
21. Hernández Guillén FJ, Janischowsky K, Ebert W, et al. (2004) Nanocrystalline diamond films for mechanical applications. *Phys Status Solidi A* 201: 2553–2557.
22. Liao MY, Meng XM, Zhou XT, et al. (2002) Nanodiamond formation by hot-filament chemical vapor deposition on carbon ions bombarded Si. *J Cryst Growth* 236: 85–89.
23. Almeida FA, Amaral M, Oliveira FJ, et al. (2007) Nano to micrometric HFCVD diamond adhesion strength to Si_3N_4. *Vacuum* 81: 1443–1447.
24. Lee HJ, Li H, Jeon H, et al. (2010) Some novel aspects of nanocrystalline diamond nucleation and growth by direct current plasma assisted chemical vapor deposition. *Diam Relat Mater* 19: 1393–1400.
25. Lisi N, Giorgi R, Dikonimos T, et al. (2010) Graphitized filament plasma enhanced CVD deposition of nanocrystalline diamond. *Diam Relat Mater* 19: 1382–1386.
26. Williams OA, Daenen M, D'Haen J, et al. (2006) Comparison of the growth and properties of ultrananocrystalline diamond and nanocrystalline diamond. *Diam Relat Mater* 15: 654–658.
27. May PW, Smith JA, Mankelevich YA (2006) Deposition of NCD films using hot filament CVD and $Ar/CH_4/H_2$ gas mixtures. *Diam Relat Mater* 15: 345–352.
28. Yang TS, Lai JY, Wong MS, et al. (2002) Substrate bias effect on the formation of nanocrystalline diamond films by microwave plasma-enhanced chemical vapor deposition. *J Appl Phys* 92: 2133–2138.
29. Faure C, Teulé-Gay L, Manaud JP, et al. (2013) Mechanisms of time-modulated polarized nano-crystalline diamond growth. *Surf Coat Technol* 222: 97–103.
30. Manaud JP, Poulon-Quintin A, Teulé-Gay L, et al. (2010) Procédé de fabrication de matériaux composites diamantés. International Patent WO/2010/076423.
31. Park JK, Lee WS, Baik YJ, et al. (2003) The pronounced grain size refinement at the edge position of the diamond-coated WC–Co inserts under microwave plasma with negative bias. *Diam Relat Mater* 12: 1657–1662.
32. Haubner R, Okoli S, Lux B (1992) The importance of the substrate surface temperature and other parameters in hot-filament diamond synthesis. *Int J Refract Met H* 11: 259–269.
33. Wei Q, Yang T, Zhou KC, et al. (2013) Effect of sputtered Mo interlayers on Si (100) substrates for the deposition of diamond film by hot filament chemical vapor deposition. *Surf Coat Technol* 232: 456–463.
34. Li YS, Tang Y, Yang Q, et al. (2010) Ultrathin W–Al Dual Interlayer Approach to Depositing Smooth and Adherent Nanocrystalline Diamond Films on Stainless Steel. *ACS Appl Mater Inter* 2: 335–338.
35. Knight DS, White WB (1989) Characterization of diamond films by Raman spectroscopy. *J Mater Res* 4: 385–393.

36. Casiraghi C, Ferrari AC, Robertson J (2005) Raman spectroscopy of hydrogenated amorphous carbons. *Phys Rev B* 72: 085401.
37. Kuzmany H, Pfeiffer R, Salk N, et al. (2004) The mystery of the 1140 cm^{-1} Raman line in nanocrystalline diamond films. *Carbon* 42: 911–917.
38. Schügerl FB, Kuzmany H (1981) Optical modes of trans-polyacetylene. *J Chem Phys* 74: 953–958.
39. Roy M, George VC, Dua AK, et al. (2002) Detection of nanophase at the surface of HFCVD grown diamond films using surface enhanced Raman spectroscopic technique. *Diam Relat Mater* 11: 1858–1862.
40. Ferrari AC, Robertson J (2004) Raman spectroscopy of amorphous, nanostructures, diamond-like carbon and nanodiamond. *Philos T R Soc A* 362: 2477–2512.
41. Klauser F, Steinmüller-Nethl D, Kaindl R, et al. (2010) Raman studies of nano- and ultra-nanocrystalline diamond films grown by hot-filament CVD. *Chem Vapor Depos* 16: 127–135.
42. Riedel R (2000) *Handbook of Ceramic Hard Materials*, Weinheim, Germany: Wiley-VCH Publishers.

AIMS Press